Fusion of Multi-Sensor Imagery for Night Vision: Color Visualization, Target Learning and Search[1]

D.A. Fay, A.M. Waxman, M. Aguilar[2], D.B. Ireland, J.P. Racamato,
W.D. Ross, W.W. Streilein, and M.I. Braun

Massachusetts Institute of Technology
Lincoln Laboratory
Lexington, MA 02420, USA
waxman@ll.mit.edu

Abstract - *We present methods and results for fusion of imagery from multiple sensors to create a color night vision capability. The fusion system architectures are based on biological models of the spatial and opponent-color processes in the human retina and visual cortex, implemented as shunting center-surround feed-forward neural networks. Real-time implementation of the dual-sensor fusion system combines imagery from either a low-light CCD camera or a short-wave infrared camera, with thermal long-wave infrared imagery. Results are also shown for extensions of this fusion architecture to include imagery from all three of these sensors, Visible/SWIR/LWIR, as well as a four sensor system using Visible/SWIR/MWIR/LWIR cameras. We also demonstrate how results from these multi-sensor fusion systems are used as inputs to an interactive tool for target designation, learning, and search based on a Fuzzy ARTMAP neural network.*

Keywords: Sensor fusion, image fusion, night vision, real-time processing, data mining, target recognition.

1 Introduction

There are a variety of sensors capable of performing under low-light conditions, imaging from the visible through the thermal infrared parts of the spectrum. Each sensor reveals different information in any given scene. The work presented here addresses the issue of combining or *fusing* this imagery, while preserving the complementary information from each band, both for visualization and as input to an in-line target learning, recognition, and tracking system.

We build upon work that we have presented over the last several years focusing on the real-time fusion of low-light visible and thermal infrared imagery [1-12]. We have also demonstrated modifications of these techniques for fusion of imagery from up to six different bands, ranging from the visible through SWIR, as well as fusion of visible, infrared and SAR (synthetic aperture radar) imagery [13,14].

Prior to our introduction of opponent-color image fusion, other methods for fusing imagery were based upon maximizing image contrasts across multiple scales via pixel comparisons and image blending [15-19]. Human factors testing has shown that the resulting gray-scale fused images do not provide the same target pop-out as our color fused results [12,20]. There are other color fusion methods that have also shown superior performance over gray-scale fusion methods for target detection, but they do so at the cost of reduced overall visual quality [20,21].

We have modified our real-time dual-sensor fusion system to work with SWIR and LWIR cameras. Imaging in the SWIR band of 0.9-1.7 microns has two primary tactical advantages over the visible band for night operations. First, the night glow of the atmosphere is significantly greater in the SWIR band than in the visible or near-IR bands on a moonless night. Second, imaging in the SWIR band has the potential to detect camouflage in the presence of foliage [13,22]. We have also initiated explorations into combining visible, SWIR and LWIR imagery, since each band contains unique and complementary information. By adding a fourth complementary band, MWIR, even more useful results can be achieved. Additionally, we have integrated into our real-time system the capability for user target designation with in-line target learning and real-time target recognition from the fused dual-band target signature. Example results will be shown using two, three and four-band fusion products as inputs to this target learning and recognition system. After describing the sensors and computing hardware used, we introduce the biological motivations and fusion system architectures. We show example multi-sensor fusion results for each of the architectures, then describe the target learning and recognition system and its performance.

2 Sensors and computing hardware

Our real-time multi-sensor imaging pod is shown in (top) Figure 1. On the lower shelf of the pod is a dual-sensor configuration consisting of an InGaAs SWIR camera from Sensors Unlimited, Inc., and an uncooled microbolometer

[1] This work was sponsored by the U.S. Defense Advanced Research Projects Agency, under Air Force Contract F19628-95-C-0002. Opinions, interpretations, conclusions, and recommendations are those of the authors and not necessarily endorsed by the U.S. Air Force.
[2] Present Address: MCIS Department, Jacksonville State University, Jacksonville, AL 36265, U.S.A.

LWIR imager from the Sanders (Lockheed Martin) Corp. The SWIR camera is sensitive from 0.9 to 1.7 microns and can output 12 bit digital data, while the LWIR imager operates in the range 7 to 13 microns and outputs 15 bit digital data. They both operate at 60 fps (frames per second) and are 320x240 pixels in resolution. The two sensors are optically registered by using a dichroic beam splitter that passes the SWIR band while reflecting the LWIR band. These two sensors feed our real-time fusion system that produces color fused results at 30 fps.

The upper shelf of the sensor pod in Figure 1 (top) supports a Lincoln Laboratory low-light CCD imager of 640x480 resolution, that outputs 12 bit digital data at 30 fps, and an MWIR InSb imager from Raytheon Amber Corp. of 256x256 resolution, that outputs 12 bits digital data at 60 fps. The low-light CCD imager is sensitive from 0.4 to 1.0 microns while the MWIR camera operates from 3 to 5 microns. These two cameras are bore-sighted to each other and to the SWIR / LWIR pod below it. These offsets are compensated for in software at the workstation when the imagery is registered off-line.

The real-time fusion processor we assembled had to be able to process two 16-bit digital input streams and perform 1.5 billion operations per second. We chose the Matrox Corp. Genesis boards because they were based on the powerful TI C80 DSP chips, and their modular architecture made the system easily expandable. The C80 processor consists of one master floating point processor and four parallel integer processors. The Genesis boards come in two versions: a main board and a co-processor board. The main board contains one C80, 16MB of SDRAM, two VIA (Video Interface ASIC) chips for independently controlling communications, an optional NOA (Neighborhood Operation Accelerator) chip, an analog/digital image grab daughter board, and a video display section. The co-processor board contains two sets of the chips on the main board, except for the data acquisition and display sections.

Our system is comprised of two Genesis main boards and two Genesis co-processor boards, in an industrial PC rack-mount chassis, with a Pentium II host processor card (see Figure 1, bottom). Digital data is input via the two daughter cards connected to the two Genesis main boards. We dedicate two C80 nodes to pre-processing each of the input streams. Pre-processing includes image warping for registration, noise cleaning, contrast enhancement, and adaptive dynamic range compression. The remaining two nodes are used to fuse the preprocessed results and drive the color display. Communication between the nodes is done over the VMChannel (VESA Media Channel), a dedicated bus separate from the PCI bus. Currently, the real-time system only supports the fusion of imagery from two sensors, but it could be expanded to accept imagery from three or four sensors and mapping the additional (similar) computations to other C80 processors.

An example image from each sensor is shown in Figure 2. These images were collected in July 1999 under 2/3-moon conditions (27mLux)) at the Lincoln Laboratory Test Range using 42° diagonal field-of-view optics. The truck and the man are about 35m from the sensors, while the trees begin at a distance of about 100m. The low-light visible CCD and the SWIR provide good detail of the truck, man, and the leaves of the trees, in addition to good separation of the vehicle from the background. In the MWIR and the LWIR images, the man in the truck becomes evident, as does a deer by the trees in the left half of the imagery. Both contain good contrast between the trees and the sky, but in the MWIR image there is also good contrast between the trees and the ground. Through our fusion process we turn the strong spatial contrasts that each sensor reveals, in conjunction with cross-sensor contrasts, into color contrasts in the final display.

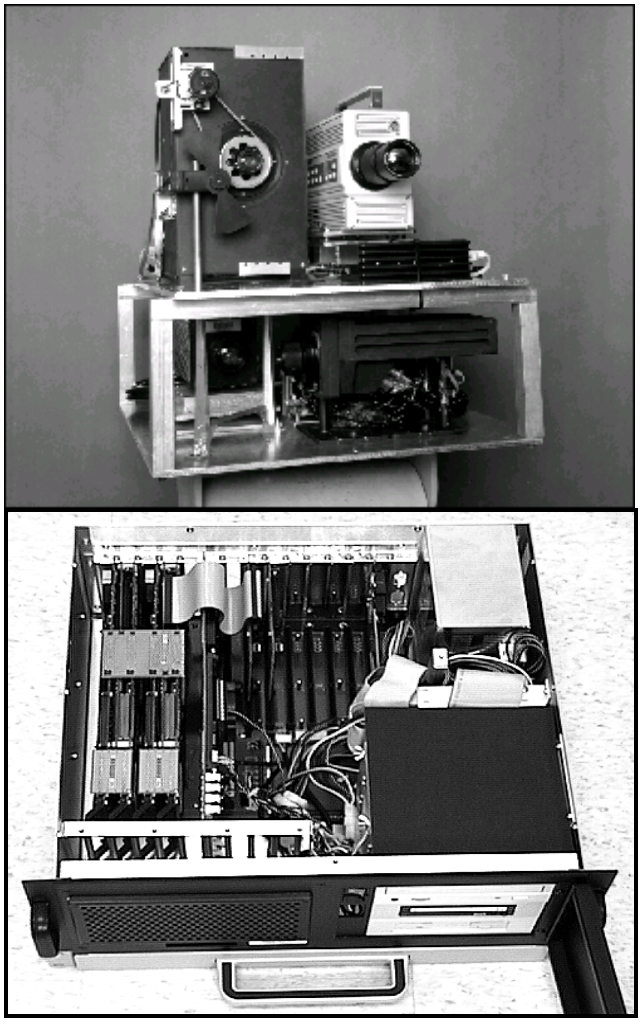

Figure 1: Multi-sensor imaging pod and real-time computing system. *(Top)* On the upper shelf, the camera on the left is the Lincoln Laboratory low-light CCD and on the right is the Raytheon Amber MWIR imager. On the lower shelf, behind the dichroic beam splitter to the left sits the Sensors Unlimited SWIR camera, and on the right is the Sanders (Lockheed Martin) LWIR imager. *(Bottom)* The industrial PC chassis contains four Matrox Genesis C80 boards (left) and a Pentium II host processor.

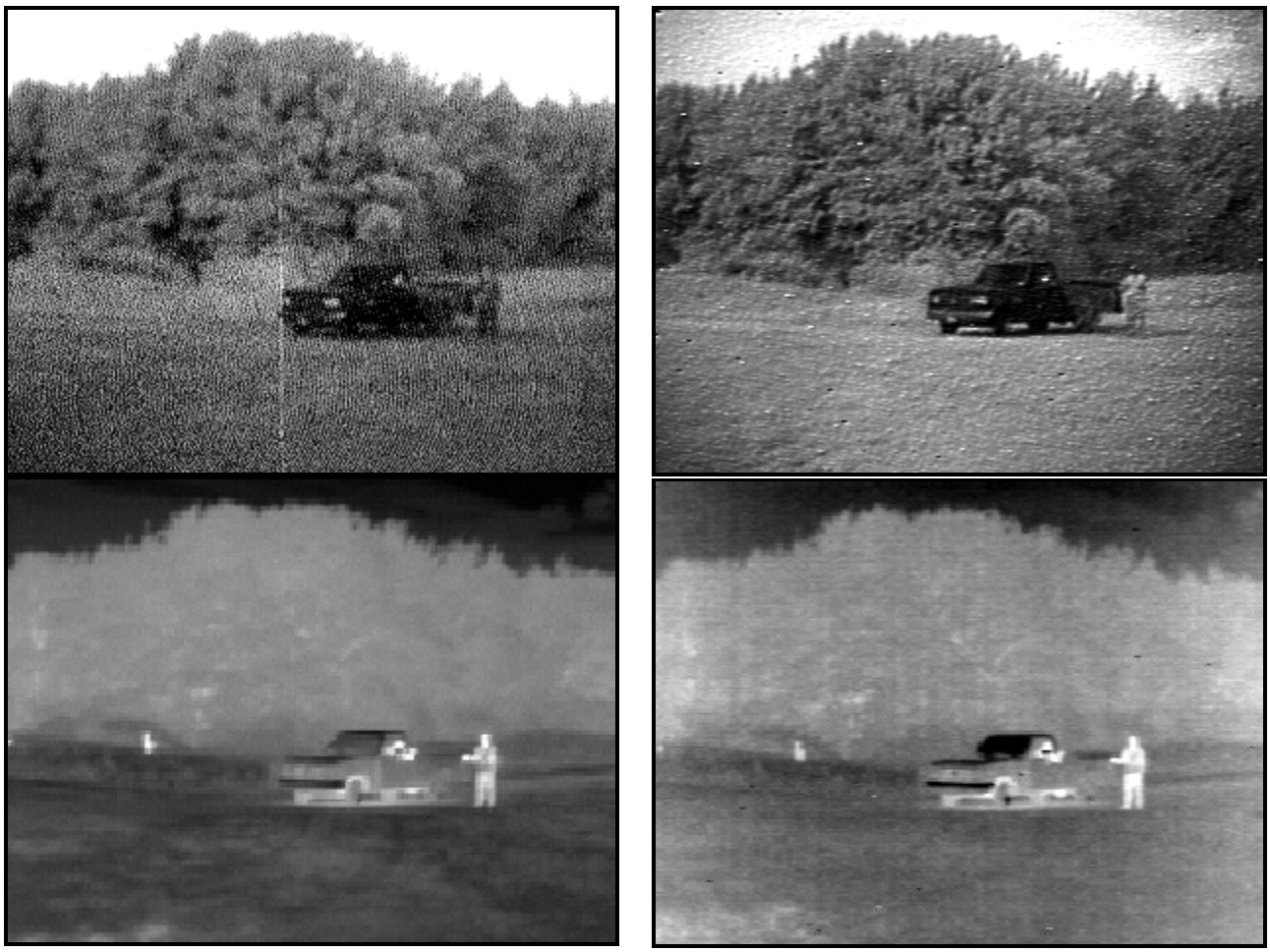

Figure 2 : Imagery from four sensors taken under 2/3-moon (27 mLux) conditions. Vehicle and man are at a distance of about 35m, while the trees start at about 100m. ***(Upper left)*** **Low-light visible;** ***(Upper right)*** **SWIR** ***(Lower left)*** **MWIR;** ***(Lower right)*** **LWIR.**

3 Biologically motivated multi-sensor image fusion

Our image fusion architectures are motivated by the biological computational processes of the human retina and the primary visual cortex. The three different cone cells in the retina are sensitive to the short, medium, and long wavelengths of the visible spectrum [23]. The outputs from these photoreceptors are then contrast enhanced within band by both ON and OFF *center-surround* spatial opponent processes at the bipolar cells [24]. In later stages (ganglion cells in retina, and V1) these signals are contrast enhanced by center-surround processes between the different bands [25,26]. This opponent-color processing separates (or decorrelates) the complementary information that each band contains. This insight into how the visual system contrasts and combines information from different spectral bands, provides one example of a working multi-spectral fusion system. Other biological fusion systems of relevance are the visible/thermal processing pathways of the rattlesnake and python [5,27,28].

In the past, we have described our architecture for fusing imagery from a low-light visible CCD camera and an uncooled LWIR imager in real-time [1-5]. We have since modified our real-time system to include a SWIR camera instead of the low-light CCD. In addition, we are now exploring the combining of imagery from three and four different spectral bands relevant to night vision applications. All the architectures utilize the center-surround feedforward shunting network [29] as a fundamental building block, for both within-band and cross-band (i.e., opponent-color) contrast enhancement.

As illustrated in Figure 3, the first stage of processing in the visible/LWIR architecture is image registration and noise cleaning. Next, each band is separately contrast enhanced and adaptively normalized by shunting center-surround processing. The LWIR image is processed by both ON-center / OFF-surround and OFF-center / ON-surround shunting networks. This treats the warm contrasts of the scene separately from the cool contrasts, since both are often equally as important. In a second stage of center-surround processing we form grayscale fused single-opponent color-contrast images. These three processes will form the red, green and blue components of the final color fused image. The enhanced ON-center LWIR (*+LWIR*) feeds the center of the red channel, while the enhanced visible (*+Vis*) feeds the inhibitory surround. The green channel gets *+Vis* in the center and both *+LWIR* and the OFF-center LWIR (*-LWIR*) in the

inhibitory surround. Finally, *-LWIR* feeds the blue channel center and the *+Vis* feeds the inhibitory surround. The net effect is a decorrelation of the sensor imagery being used to drive the displayed color contrasts. An optional final step is to convert the *RGB* image into *HSV* color space, then remap the hue values of the entire image by means of a user controlled rotation of the hue circle. This can be done to provide a more natural coloring to the background scene while maintaining target pop-out.

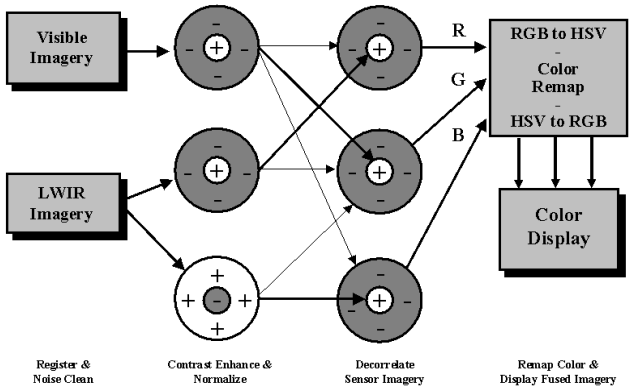

Figure 3 : Low-light visible / LWIR neural network fusion architecture

The main modification to the architecture of Figure 3 when applied to SWIR / LWIR fusion, as shown in Figure 4, is the addition of an intermediate center-surround processing stage that enhances a combination of the imagery from the two sensors. Each of the three enhanced results from the first stage of processing is contrasted with this *broad band* average image (*+Avg*). The comparison of the SWIR processed result with this average image drives the green channel. The red channel is the contrast of *+LWIR* with respect to *+Avg* and the blue channel is the contrast of *–LWIR* with *+Avg*. In this dual-band architecture, the color contrasts are driven by how each band (SWIR, warm LWIR, cool LWIR) differs from the average.

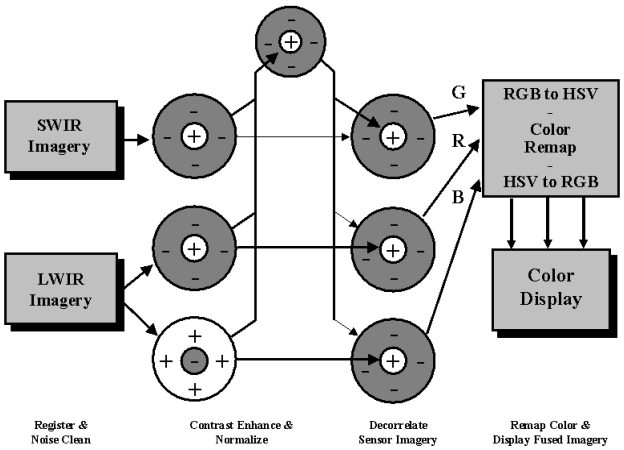

Figure 4 : SWIR / LWIR fusion architecture

There are two major differences between the dual-sensor architectures and the tri- and quad-sensor architectures of Figures 5 and 6 [13,14]. The first is the addition of a third layer of processing during the decorrelation phase, motivated by the double-opponent color processing cells in the primary visual cortex. The second is the mapping of the gray-scale fused outputs to *YIQ* color space, instead of *RGB*. This change was driven by the fact that there are now two sets of paired results from the first stage of decorrelation. The *YIQ* model is a simple approximation to human opponent-color perception and is employed in commercial color TV broadcasting; *Y* represents the brightness, *I* the red-green contrast, and *Q* the blue-yellow contrast channels. In the case of the tri-sensor fusion architecture, the double-opponent result from the *+Vis-LWIR* combination feeds the *I* channel, while the result from *+SWIR+LWIR* drives the *Q* channel. Due to these combinations, contrasts between the visible and LWIR will show up as red-green color contrast. Likewise, contrast between the SWIR and LWIR will be seen as blue-yellow color contrasts. The quad-sensor architecture replaces the *–LWIR* with the contrast enhanced MWIR. The pairings are chosen to maximize the complementary information between the reflective and emissive bands.

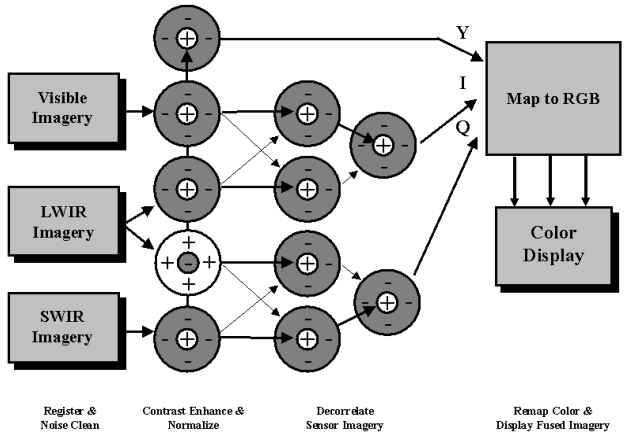

Figure 5 : Visible/SWIR/LWIR fusion system

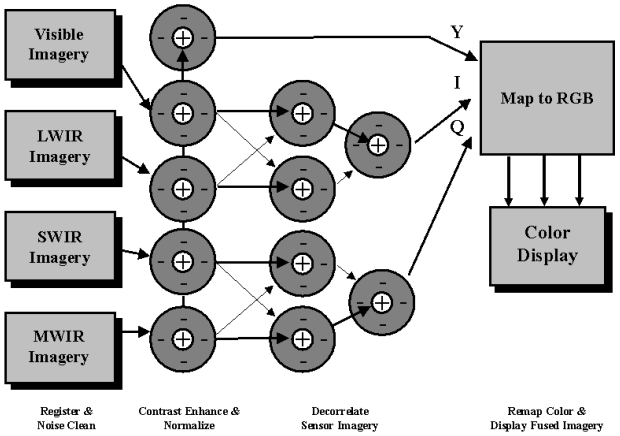

Figure 6 : Visible/SWIR/MWIR/LWIR fusion

Example results from the four different sensor fusion architectures are shown in Figure 7. All four scenes have a natural appearance with good color contrast between the men, vehicles, background vegetation, and sky. The low-light visible / LWIR color fused result shows good separation between the trees, sky and grass, but does not provide good contrast between parts of the truck and the grass. The SWIR / LWIR fusion system provides strong

color contrast between the truck and grass, but not between the trees and grass. The low-light Visible / SWIR / LWIR fused result is able to capture the best of both systems by maintaining the strong contrasts between sky, trees, truck, and grass. Adding MWIR imagery in for quad-sensor fusion segments the scene further, e.g., the grass from the trees, and also creates the most natural appearing "daytime-like" image of the four results. Recall that these images were taken at night under 2/3-moon conditions.

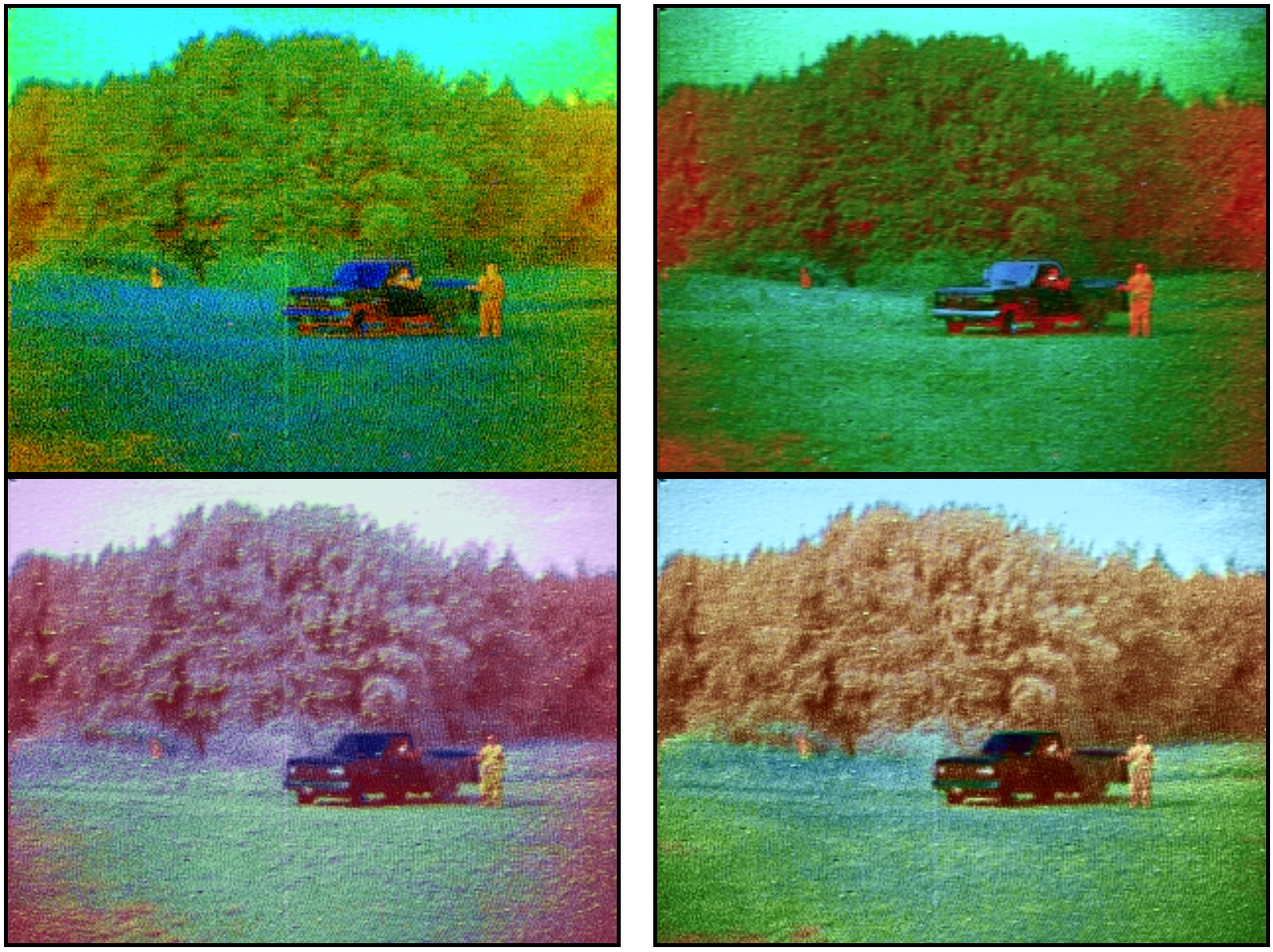

Figure 7 : Results from the four fusion nets. ***(Upper left)*** **Visible/LWIR;** ***(Upper right)*** **SWIR/LWIR;** ***(Lower left)*** **Visible/SWIR/LWIR;** ***(Lower right)*** **Visible/SWIR/MWIR/LWIR.**

4 Target learning and search

The results from multi-spectral fusion are not only useful for visualization, but also for target learning and recognition. We have developed an interactive, real-time image mining system for target learning and search in multi-sensor imagery. The system is built around the Fuzzy ARTMAP neural network [30,31,34,35]. For each sensor fusion architecture, the results from all stages of processing are combined to form a data cube, where each pixel represents a feature vector that serves as input to the Fuzzy ARTMAP classifier. Other image planes containing processed results can be added to the data cube, and hence, the approach easily accommodates other registered sensor data, e.g., other bands or 3D data.

The user is provided with a Java-coded graphical interface that allows him to select example (target) and counter-example (non-target) pixels from the color fused image. These feature vectors serve as the training set to the neural classifier. A preliminary search on a subset of the image can be performed to determine if the network is trained to satisfaction. If not, more examples and counter-examples can be selected in an iterative process. This process takes only seconds to execute. Once satisfied, the whole image can be searched. Pixels classified as targets are highlighted based on the confidence level of the network. Since the order of presentation of the input vectors is important to Fuzzy ARTMAP, multiple networks are trained with different ordered sets of inputs. The networks then vote on whether a given pixel should be classified as a target or a non-target. The voter consensus determines the degree of confidence in the classification of a given pixel. The system also uses an algorithm that examines the overlap between example and counter-example feature vectors in determining which components of the input feature vectors are necessary to achieve correct classification of the training set [33,35]. This reduced feature vector embodies a differential signature of the target with respect to the context. When

performing target search on subsequent frames of fused imagery, only those components are used, significantly speeding up the search process. Currently, we can display a search result on a new frame once every few seconds (with search implemented on a Pentium II processor). This system can be used for both tracking targets over time and for detecting their arrivals and departures from the scene. Multiple search agents can be trained to search for multiple target types on each frame.

Figure 8 shows example search results from the four fusion architectures described in the previous section. In these examples the targets were the men in the scene. Only the man standing on the right was trained upon, not the man in the truck. The results highlight the man standing, the man in the truck, but not the deer in the background. The dual-sensor systems are not able to separate the human targets from hot parts in the undercarriage of the truck. However, by adding in a third or fourth sensor, that difference is realized. Men targets can then be detected and tracked as they move about the scene.

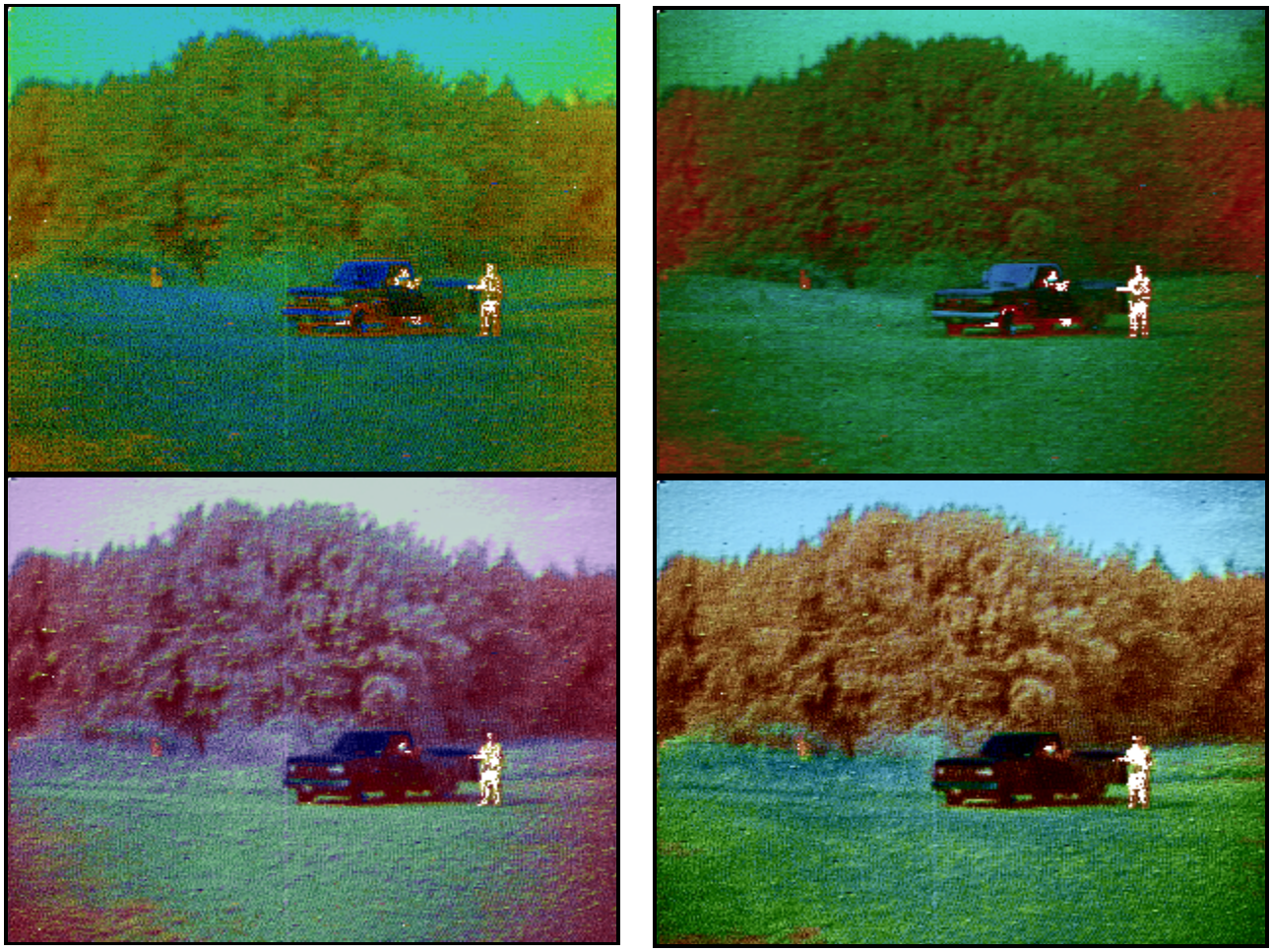

Figure 8 : Interactive target designation, learning and search results for man-targets from the four different multi-sensor fusion architectures. As more bands (i.e., sensors) are added, the search results become refined. ***(Upper)*** **Visible/LWIR [left]; SWIR/LWIR [right];** ***(Lower)*** **Visible/SWIR/LWIR [left]; Visible/SWIR/MWIR/LWIR [right].**

5 Summary

We have developed and demonstrated four multi-sensor image fusion systems for visualization, target learning and search, based upon biological models of the human visual system. A real-time, color night vision system, based on commercial DSP boards, for fusing low-light visible and LWIR, or SWIR and LWIR imagery at 30 frames/sec was described. The real-time fusion architecture, based upon a single nonlinear image processing operator, has been adapted to process imagery from more than two sensors. The resulting imagery from these fusion systems is used both for visualization and as input to an interactive tool for target learning and search. In related work, we have made use of this same approach to combine and exploit remotely sensed visible, thermal IR, synthetic aperture radar, multispectral and hyperspectral imagery in the context of 3D site models [32-35].

References

[1] M. Aguilar, D.A. Fay, D.B. Ireland, J.P. Racamato, W.D. Ross, and A.M. Waxman, "Field Evaluations of Dual-Band Fusion for Color Night Vision," *Proc. of SPIE Conf. On Enhanced and Synthetic Vision 1999*, **SPIE-3691**, pp. 168-175, 1999.

[2] M. Aguilar, D.A. Fay, W.D. Ross, A.M. Waxman, D.B. Ireland, and J.P. Racamato, "Real-time fusion of low-light CCD and uncooled IR imagery for color night vision," *Proc. of SPIE Conf. On Enhanced and Synthetic Vision 1998*, **SPIE-3364**, 1998.

[3] R.K. Reich, B.E. Burke, W. M. McGonagle, D.M. Craig, A.M. Waxman, E.D. Savoye, J.A. Gregory, and B.B. Kosicki, "Low-light-level 640x480 CCD camera for night vision application," *Proc. of the Meeting of the IRIS Specialty Group on Passive Sensors 1998*, Vol. 1, pp. 261-271, 1998.

[4] A.M. Waxman, M. Aguilar, D.A. Fay, D.B. Ireland, J.P. Racamato, W.D. Ross, J.E. Carrick, A.N. Gove, M.C. Seibert, E.D. Savoye, R.K. Reich, B.E. Burke, W.H. McGonagle, and D.M. Craig, "Solid state color night vision: Fusion of low-light visible and thermal IR imagery," *Lincoln Laboratory Journal*, **11** (1), pp. 41-60, 1998.

[5] A.M. Waxman, A.N. Gove, D.A. Fay, J.P. Racamato, J.E. Carrick, M.C. Seibert and E.D. Savoye, "Color Night Vision: Opponent Processing in the Fusion of Visible and IR Imagery," *Neural Networks*, **10** (1), pp. 1-6, 1997.

[6] A.M. Waxman, A.N. Gove, D.A. Fay, J.P. Racamato, J. Carrick, M.C. Seibert, E.D. Savoye, B.E. Burke, R.K. Reich, W.H. McGonagle, and D.M. Craig, "Solid state color night vision: Fusion of low-light visible and thermal IR imagery," *Proc. of the Meeting of the IRIS Specialty Group on Passive Sensors 1996*, **II**, pp. 263-280, 1996.

[7] A.M. Waxman, A.N. Gove, M.C. Seibert, D.A. Fay, J.E. Carrick, J.P. Racamato, E.D. Savoye, B.E. Burke, R.K. Reich, W.H. McGonagle, and D.M. Craig, "Progress on Color Night Vision: Visible/IR Fusion, Perception & Search, and Low-Light CCD Imaging," *Proc. SPIE Conf. on Enhanced and Synthetic Vision 1996*, **SPIE-2736**, pp. 96-107, 1996.

[8] A.M. Waxman, D.A. Fay, A.N. Gove, M.C. Seibert, J.P. Racamato, J.E. Carrick and E.D. Savoye, "Color night vision: Fusion of intensified visible and thermal IR imagery," *Synthetic Vision for Vehicle Guidance and Control*, **SPIE-2463**, pp. 58-68, 1995.

[9] A.M. Waxman, A.N. Gove, D.A. Fay, and J.E. Carrick, "Real-Time Adaptive Digital Image Processing for Dynamic Range Remapping of Imagery Including Low-light-level Visible Imagery," *U.S. Patent 5,909,244*, issued 6/1/99 (filed 9/5/96); rights assigned to the MIT, 1999.

[10] E.D. Savoye, A.M. Waxman, R.K. Reich, B.E. Burke, J.A. Gregory, W.H. McGonagle, A.H. Loomis, B.B Kosicki, R.W. Mountain, A.N. Gove, D.A. Fay, J.E. Carrick, "Low-light-level Imaging and Image Processing," *U.S. Patent 5,880,777*, issued 3/9/99 (filed 4/15/96); rights assigned to the MIT, 1999.

[11] A.M. Waxman, D.A. Fay, A.N. Gove, M.C. Seibert, and J.P. Racamato, "Method and apparatus for generating a synthetic image by the fusion of signals representative of different views of the same scene," *U.S. Patent 5,555,324*, issued 9/10/96 (filed 11/1/94); rights assigned to the MIT, 1996.

[12] A. Toet, J. K. IJspeert, A. M. Waxman, and M. Aguilar, "Fusion of visible and thermal imagery improves situational awareness," *Proc. SPIE Conf. on Enhanced and Synthetic Vision*, **SPIE-3088**, pp. 177-188, 1997.

[13] A.M. Waxman, M. Aguilar, R.A. Baxter, D.A. Fay, D.B. Ireland, J.P. Racamato, and W.D. Ross, "Opponent-color fusion of multisensor imagery: Visible, IR and SAR," *Proc. of the Meeting of the IRIS Specialty Group on Passive Sensors 1998*, **I**, pp. 43-61, 1998.

[14] A.N. Gove, R.K. Cunningham, and A.M. Waxman, "Opponent-color visual processing applied to multispectral infrared imagery," *Proc. of the Meeting of the IRIS Specialty Group on Passive Sensors 1996*, **II**, pp. 247-262, 1996.

[15] P.J. Burt and R.J. Kolczynski, "Enhanced image capture through fusion," *Fourth Internat'l Conf. on Computer Vision*, pp. 173-182. Los Alamitos: IEEE Computer Society Press, 1993.

[16] D. Ryan and R. Tinkler, "Night pilotage assessment of image fusion," *Helmet- and Head-Mounted Displays and Symbology Design Requirements II*, **SPIE-2465**, pp. 50-67, 1995.

[17] A. Toet, "Hierarchical image fusion," *Machine Vision and Applications*, **3**, pp. 1-11, 1990.

[18] A. Toet, "Multiscale contrast enhancement with applications to image fusion," *Optical Eng.*, **31**, 1026-1031, 1992.

[19] A. Toet, L.J. van Ruyven and J.M. Valeton, "Merging thermal and visual images by a contrast pyramid," *Optical Eng.*, **28**, pp. 789-792, 1989.

[20] P.M. Steele and P. Perconti, "Part task investigation of multispectral image fusion using gray scale and synthetic color night vision sensor imagery for helicopter pilotage," *Targets and Backgrounds: Characterization and Representation III*, **SPIE-3062**, pp. 88-100, 1997.

[21] A. Toet and J. Walraven, "New false color mapping for image fusion," *Optical Engineering*, **35**, pp. 650-658, 1996.

[22] M. Norton, R. Kindsfather, and R. Dixon, "Short-wave (1-2.8 μm) imagery applications for fun and profit," *Terrorism and Counterterrorism Methods and Technologies*, **SPIE-2933**, pp. 9-31, 1997.

[23] P.K. Kaiser and R.M. Boynton, **Human Color Vision,** Optical Society of America, Washington, DC, 1996.

[24] P. Schiller, "The ON and OFF channels of the visual system," *Trends in Neuroscience*, **TINS-15**, pp. 86-92, 1992.

[25] P. Schiller and N.K. Logothetis, "The color-opponent and broad-band channels of the primate visual system," *Trends in Neuroscience*, **TINS-13**, pp. 392-398, 1990.

[26] P. Gouras, "Color Vision," Chapter 31 in **Principles of Neural Science** (E.R. Kandel, J.H. Schwartz, and T.M. Jessell, editors), pp. 467-480, New York: Elsevier Science Publishers, 1991.

[27] E.A. Newman and P.H. Hartline, "The infrared vision of snakes," *Scientific American*, **246** (March), pp. 116-127, 1982.

[28] E.A. Newman and P.H. Hartline, "Integration of visual and infrared information in bimodal neurons of the rattlesnake optic tectum," *Science*, **213**, pp. 781-791, 1981.
[29] S.A. Ellias and S. Grossberg,, "Pattern formation, contrast control, and oscillations in the short memory of shunting on-center off-surround networks," *Biological Cybernetics*, **20**, pp. 69-98, 1975.
[30] G.A. Carpenter, S. Grossberg, N. Markuzon, J.H. Reynolds, and D.B. Rosen, "Fuzzy ARTMAP: A neural network architecture for incremental supervised learning of analog multidimensional maps," *IEEE Transactions on Neural Networks*, **3**, pp. 698-713, 1992.
[31] T. Kasuba, "Simplified Fuzzy ARTMAP", *AI Expert*, Nov 1993.
[32] W. Ross, A. Waxman, W. Streilein, J. Verly, F. Liu, M. Braun, P. Harmon, and S. Rak, "Multi-sensor image fusion for efficient color 3D site visualization and rapid analysis utilizing search acceleration algorithms," to appear in *Proc. of the Fourth International Conference on Cognitive and Neural Systems*, Boston, MA, May 24-27, 2000.
[33] W. Streilein, A. Waxman, W. Ross, M. Braun, F. Liu, and J. Verly, "An interactive mining tool utilizing an extension of Fuzzy ARTMAP for efficient exploitation and enhanced visualization of multi-sensor imagery," to appear in *Proc. of the Fourth International Conference on Cognitive and Neural Systems*, Boston, MA, May 24-27, 2000.
[34] W. Ross, A. Waxman, W. Streilein, J. Verly, F. Liu, M. Braun, P. Harmon, and S. Rak, "Multi-sensor image fusion for 3D site visualization and search," to appear in *Proc. of the Third International Conference on Information Fusion*, Paris, July 10-13, 2000.
[35] W. Streilein, A. Waxman, W. Ross, F. Liu, M. Braun, J. Verly, and Read, "Fused multi-sensor image mining for feature foundation data," to appear in *Proc. of the Third International Conference on Information Fusion*, Paris, July 10-13, 2000.